

Raman and infrared spectra of complex low energy tetrahedral carbon allotropes from first-principles calculations

Hui Wang(王翬), Ze-Yu Zhang(张泽宇), Xiao-Wu Cai(蔡小五), Zi-Han Liu(刘子晗), Yong-Xiang Zhang(张永翔), Zhen-Long Lv(吕珍龙), Wei-Wei Ju(琚伟伟), Hui-Hui Liu(刘汇慧), Tong-Wei Li(李同伟), Gang Liu(刘钢), Hai-Sheng Li(李海生), Hai-Tao Yan(闫海涛), Min Feng(冯敏)

Citation: Chin. Phys. B . 2020, 29(9): 093601 . **doi:** 10.1088/1674-1056/ab9613
Journal homepage: http://cpb.iphy.ac.cn; http://iopscience.iop.org/cpb

What follows is a list of articles you may be interested in

Dependence of mechanical properties on the site occupancy of ternary alloying elements in γ'-Ni_3Al: *Ab initio* description for shear and tensile deformation

Minru Wen(文敏儒), Xing Xie(谢兴), Huafeng Dong(董华锋), Fugen Wu(吴福根), Chong-Yu Wang(王崇愚)

Chin. Phys. B . 2020, 29(7): 078103 . **doi:** 10.1088/1674-1056/ab8a38

Prediction of structured void-containing 1T-$PtTe_2$ monolayer with potential catalytic activity for hydrogen evolution reaction

Bao Lei(雷宝), Yu-Yang Zhang(张余洋), Shi-Xuan Du(杜世萱)

Chin. Phys. B . 2020, 29(5): 058104 . **doi:** 10.1088/1674-1056/ab8203

Modulation of magnetic and electrical properties of bilayer graphene quantum dots using rotational stacking faults

Hong-Ping Yang(杨宏平), Wen-Juan Yuan(原文娟), Jun Luo(罗俊), Jing Zhu(朱静)

Chin. Phys. B . 2019, 28(7): 078106 . **doi:** 10.1088/1674-1056/28/7/078106

Structural evolutions and electronic properties of Au_nGd (n=6-15) small clusters: A first principles study

Han-Xing Zhang(张汉星), Chao-Hao Hu(胡朝浩), Dian-Hui Wang(王殿辉), Yan Zhong(钟燕), Huai-Ying Zhou(周怀营), Guang-Hui Rao(饶光辉)

Chin. Phys. B . 2018, 27(8): 083601 . **doi:** 10.1088/1674-1056/27/8/083601

Influence of Ni on Cu precipitation in Fe–Cu–Ni ternary alloy by an atomic study

Zhu Lu-Shan, Zhao Shi-Jin

Chin. Phys. B . 2014, 23(6): 063601 . **doi:** 10.1088/1674-1056/23/6/063601

Raman and infrared spectra of complex low energy tetrahedral carbon allotropes from first-principles calculations*

Hui Wang(王翬)[1,†], Ze-Yu Zhang(张泽宇)[1], Xiao-Wu Cai(蔡小五)[2], Zi-Han Liu(刘子晗)[1], Yong-Xiang Zhang(张永翔)[1,3], Zhen-Long Lv(吕珍龙)[1], Wei-Wei Ju(琚伟伟)[1], Hui-Hui Liu(刘汇慧)[1], Tong-Wei Li(李同伟)[1], Gang Liu(刘钢)[1], Hai-Sheng Li(李海生)[1], Hai-Tao Yan(闫海涛)[1], and Min Feng(冯敏)[4,‡]

[1] *Henan Key Laboratory of Photoelectric Energy Storage Materials and Applications, School of Physics Engineering, Henan University of Science and Technology, Luoyang* 471023, *China*

[2] *First High School of Luoyang City, Luoyang* 471001, *China*

[3] *Institute of Microelectronics of Chinese Academy of Sciences, Beijing* 100029, *China*

[4] *School of Physics, Nankai University, Tianjin* 300071, *China*

(Received 31 March 2020; revised manuscript received 20 May 2020; accepted manuscript online 25 May 2020)

Up to now, at least 806 carbon allotropes have been proposed theoretically. Three interesting carbon allotropes (named *Pbam*-32, *P*6/*mmm*, and $I\bar{4}3d$) were recently uncovered based on a random sampling strategy combined with space group and graph theory. The calculation results show that they are superhard and remarkably stable compared with previously proposed metastable phases. This indicates that they are likely to be synthesized in experiment. We use the factor group analysis method to analyze their Γ-point vibrational modes. Owing to their large number of atoms in primitive unit cells (32 atoms in *Pbam*-32, 36 atoms in *P*6/*mmm*, and 94 atoms in $I\bar{4}3d$), they have many Raman- and infrared-active modes. There are 48 Raman-active modes and 37 infrared-active modes in *Pbam*-32, 24 Raman-active modes and 14 infrared-active modes in *P*6/*mmm*, and 34 Raman-active modes and 35 Raman- and infrared-active modes in $I\bar{4}3d$. Their calculated Raman spectra can be divided into middle frequency range from 600 cm^{-1} to 1150 cm^{-1} and high frequency range above 1150 cm^{-1}. Their largest infrared intensities are 0.82, 0.77, and 0.70 $(D/Å)^2$/amu for *Pbam*, *P*6/*mmm*, and $I\bar{4}3d$, respectively. Our calculated results provide an insight into the lattice vibrational spectra of these sp^3 carbon allotropes and suggest that the middle frequency Raman shift and infrared spectrum may play a key role in identifying newly proposed carbon allotropes.

Keywords: Raman and infrared spectra, carbon allotrope, first-principles calculation

PACS: 36.20.Ng, 81.05.U–, 63.20.dk **DOI:** 10.1088/1674-1056/ab9613

1. Introduction

The unique ability of carbon element to form sp, sp^2, and sp^3 hybridized bonds leads to a large number of allotropes.[1] Among them, diamond (three dimensions), graphene (two dimensions), carbon nanotubes (one dimension), and fullerene (zero dimension) have been widely investigated in various applications. They can be insulator, semiconductor, semimetal, metal or even superconductor.[2,3] This made carbon allotrope prediction to be a very active field of investigation in recent years.[4–7] As shown in Samara Carbon Allotrope Database, at least 522 three-dimensional carbon allotropes have been proposed based on a variety of sophisticated algorithms.[1] Among these newly proposed carbon allotropes, some of them (C20-sc, C21-sc, C22-sc,[8,9] M carbon,[6,10] S carbon,[11,12] T carbon,[13,14] V carbon,[15] and Z carbon[16]) are reported to be obtained in experiment. However, not all experiments can be explained by these proposed carbon allotropes. For example, diamond anvil can even be indented by cold-compressed graphite, but its structure is still totally unresolved.[17]

Multi-scale computation simulation is often used for searching and investigating new materials.[18] The energy surface of carbon is very complex, especially for crystals with large unit cell. In order to meet this challenge, Shi *et al.*[5] and He *et al.*[7] uncovered 284 carbon allotropes with a random sampling strategy combined with space group and graph theory. This method enables the search for large-size and complex carbon allotropes up to 100 carbon atoms per unit cell. After a systematical search for large-size sp^3 carbon crystals, three complex low energy tetrahedral carbon allotropes (*Pbam*-32, *P*6/*mmm*, and $I\bar{4}3d$) were uncovered recently, and the calculated phonon dispersions and elastic constants show that they are dynamically and mechanically stable.[7] There are 32, 36, and 94 atoms in their primitive unit cells, respectively and their energy relative to diamond is 0.10 eV/atom for *Pbam*-32, 0.13 eV/atom for *P*6/*mmm*, 0.14 eV/atom for $I\bar{4}3d$. The relative energy of other metastable carbon allotropes is 0.11 eV/atom for C-carbon, 0.14 eV/atom for T12, 0.15 eV/atom for Z-carbon, 0.15 eV/atom for P-

*Project supported by the National Natural Science Foundation of China (Grant Nos. U1404111, 11504089, 61874160, 61675064, and 11404098), the Fund for Young Key Teacher of Henan Province, China (Grant No. 2016GGJS-059), and the Henan Provincial Major Scientific and Technological Projects, China (Grant No. 182102210289).

†Corresponding author. E-mail: nkxirainbow@gmail.com

‡Corresponding author. E-mail: nkfm@nankai.edu.cn

© 2020 Chinese Physical Society and IOP Publishing Ltd

carbon, 0.16 eV/atom for O-carbon, 0.18 eV/atom for W-c arbon, 0.19 eV/atom for M-carbon, 0.19 eV/atom for F-carbon, 0.21 eV/atom for X-carbon, and 0.23 eV/atom for Bct-C4. Therefore, these three newly proposed carbon allotropes are remarkably stable compared with those metastable phases previously proposed, which indicates that they are very likely to be synthesized in experiment. Furthermore, the $I\bar{4}3d$ structure has the widest electronic band gap of 7.25 eV in carbon allotrope family.

In the investigation of carbon materials, Raman spectrum, as a fast, cheap and nondestructive method, plays a key role in identifying them.[19–23] For example, the D, G, and 2D peaks of graphene,[22,24–26] the interlay shearing and breathing mode of multilayer graphene,[20,21,27] the breathing mode of carbon nanotube[28,29] provide unique fingerprint of them. Besides Raman spectrum, infrared spectrum is also widely used to characterize carbon nanotube,[30] graphite,[31] graphene,[32] and even diamond under electric field.[33] In order to investigate the first order Raman and infrared spectra of these three newly proposed carbon allotropes, we perform factor group analysis and first-principles calculation and obtain their Raman tensor and infrared intensity of Γ-point vibrational modes.

2. Calculation method

All the density-functional calculation was obtained under the framework of the local density approximation (LDA) as implemented in the Quantum Espresso package.[34] The wave function was expanded in a plane-wave basis set with an energy cutoff of 100 Ry (1 Ry = 13.6056923(12) eV). The k-points in the Brillouin zone of the primitive unit cell were sampled on 4×4×10 mesh for *Pbam*-32, 4×4×10 mesh for $P6/mmm$, and 4×4×4 mesh for $I\bar{4}3d$. The Monkhorst–Pack k-mesh was employed for the Brillouin-zone integration. The norm-conserving pseudopotential was used to represent the electron–ion interaction.[35] The Γ-point vibrational frequency, Raman activity, and infrared intensity were calculated within the framework of density functional perturbation theory.[36–40]

3. Results and discussion

3.1. Crystal structure and symmetry

The crystal structure of *Pbam*-32, $P6/mmm$, and $I\bar{4}3d$ are depicted in Fig. 1. The *Pbam*-32 has 32 carbon atoms in its primitive unit cell with a two-fold ration axis along $\boldsymbol{a}_3$ direction. As shown in Fig. 1(a), the primitive unit cell is composed of fivefold, sixfold and sevenfold topological carbon rings. As it can be easily transformed from wrinkled graphite, *Pbam*-32 is a good candidate product of cold compressed graphite. The $P6/mmm$ has 36 carbon atoms in its primitive unit cell with a six-fold ration axis along $\boldsymbol{a}_3$ direction. As depicted in Fig. 1(b), the fivefold and sixfold carbon rings arrange around the center eightfold carbon rings in $P6/mmm$. Unlike *Pbam*-32, $P6/mmm$ cannot be obtained by simply transformation from graphite. However, it can be acquired from well-arranged array of certain carbon nanotubes.

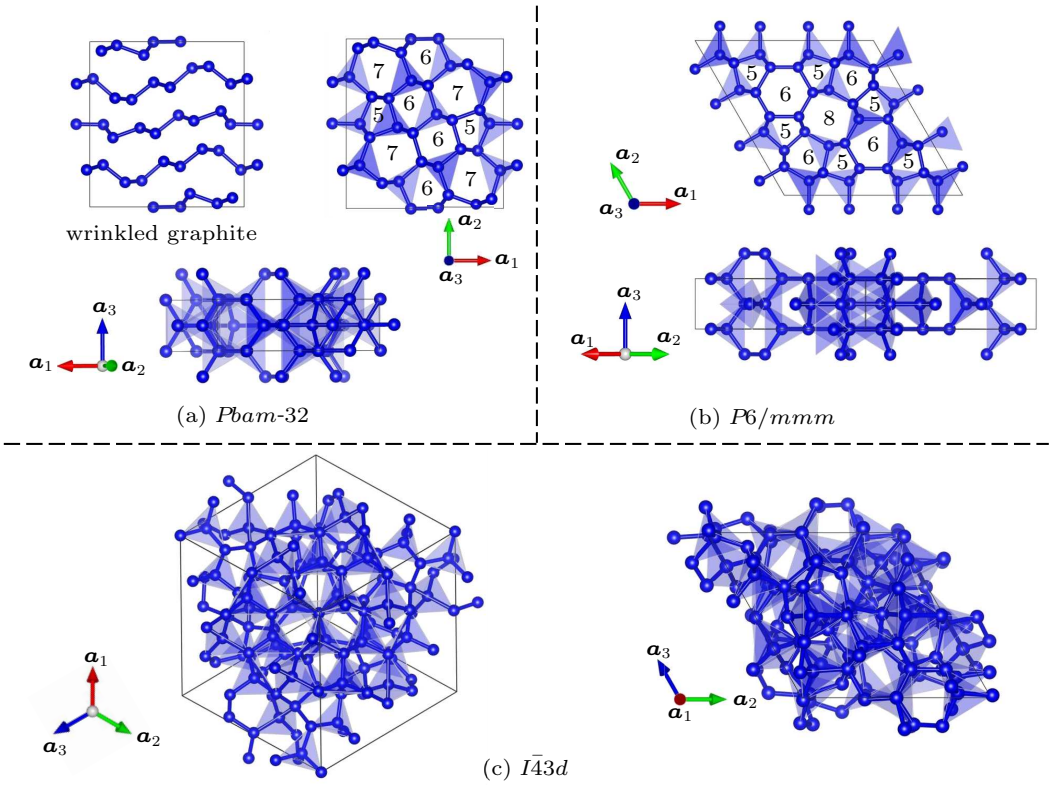


Fig. 1. Primitive cell of (a) *Pbam*-32, (b) $P6/mmm$, and (c) $I\bar{4}3d$. They are composed of tetrahedra network, which is the characteristic of sp^3 hybridization. The numbers of panels (a) and (b) refer to fivefold, sixfold, sevenfold, and eightfold topological carbon rings.

As shown in Fig. 1(c), the structure of $I\bar{4}3d$ is cubic, containing 94 carbon atoms in its primitive unit cell. Due to its complexity, $I\bar{4}3d$ can be obtained neither from graphite nor from carbon nanotubes directly. It might be synthesized in explosive shock experiment. It can be seen from Fig. 1 that the carbon atoms of *Pbam*-32 form tetrahedron network, and so do those of $P6/mmm$ and $I\bar{4}3d$. A carbon atom has six electrons with a $(1s)^2(2s)^2(2p)^2$ configuration. The energy difference between the 2s- and the 2p-states is small. Therefore, in molecular or crystal, it is possible to excite one carbon electron from the 2s-state into the 2p-state. This results in a special state: one s-orbital and three p-orbitals. These four orbitals form the sp^3 hybridization. The direction of the sp^3 hybridization makes a carbon form a tetrahedral assembly with its neighbors, like diamond. It is the characteristic of sp^3 hybridization. As *Pbam*-32 and $P6/mmm$ have the inversion center symmetry, they have neither piezoelectric nor second harmonic generation response.[41,42] The calculated lattice parameters and relative energy values are listed in Table 1.

Their Γ-point vibrational modes are classified with the factor group analysis method.[43] Owing to the inversion center symmetry, the vibrational modes of *Pbam*-32 and $P6/mmm$ are either 'g' mode or 'u' mode. All the optical vibrational modes at Γ-point are listed in Table 2. Owing to its low symmetry, *Pbam*-32 has only non-degenerate modes. Therefore, it has 96 (3×32) non-degenerate vibrational modes at Γ point. There are three translational modes (B_{1u}, B_{2u}, and B_{3u}) among them. The other 93 vibrational modes are optical modes. There are 48 Raman-active modes ($16A_g+16B_{1g}+8B_{2g}+8B_{3g}$), 37 infrared-active modes ($7B_{1u}+15B_{2u}+15B_{3u}$), and 8 silent modes ($8A_u$). Owing to the six-fold rotation symmetry, $P6/mmm$ has doubly degenerate modes. It has one non-degenerate translational mode (A_{2u}) and one doubly degenerate translational mode (E_{1u}). Besides, it has 24 Raman-active modes ($6A_{1g}+6E_{1g}+12E_{2g}$), 14 infrared-active modes ($3A_{2u}+11E_{1u}$), and 32 silent modes ($2A_{1u}+6A_{2g}+4B_{1g}+2B_{2g}+6B_{1u}+6B_{2u}+6E_{2u}$). Owing to its high symmetry, $I\bar{4}3d$ has triply degenerate mode. It has a triply degenerate translational mode T_2. Besides, it has 34 Raman-active modes ($11A_1+23E$) and 47 silent modes ($12A_2+35T_1$). Unlike the other two crystals, $I\bar{4}3d$ has 35 T_2 modes, which are both Raman- and infrared-active.

Table 1. Calculated crystal parameters of *Pbam*-32, $P6/mmm$, and $I\bar{4}3d$. Integer fractions represent atomic positions fixed by symmetry. Their energy values relative to diamond are listed in the last column. Data with * is cited from Ref. [7].

Structure	*a*/Å	*b*/Å	*c*/Å	Atomic positions	Energy/(eV/atom)
Pbam-32	8.193 8.303*	8.145 8.865*	2.484 2.511*	4*h* (0.088 0.499 1/2) 4*h* (0.837 0.341 1/2) 4*h* (0.575 0.555 1/2) 4*h* (0.480 0.276 1/2) 4*g* (0.729 0.351 0) 4*g* (0.850 0.580 0) 4*g* (0.174 0.979 0) 4*g* (0.586 0.245 0)	0.10
$P6/mmm$	9.738 9.855*	9.738 9.855*	2.471 2.497*	6*l* (0.093 0.185 0) 6*m* (0.145 0.290 1/2) 12*p* (0.828 0.336 0) 12*q* (0.090 0.410 1/2)	0.13
$I\bar{4}3d$	10.126 10.289*	10.126 10.289*	10.126 10.289*	12*b* (0 3/4 5/8) 16*c* (0.757 0.743 0.257) 16*c* (0.852 0.648 0.352) 48*e* (0.893 0.555 0.584) 48*e* (0.450 0.381 0.705) 48*e* (0.254 0.417 0.426)	0.14

Table 2. Γ-point optical vibrational modes of *Pbam*-32, $P6/mmm$, and $I\bar{4}3d$.

Structure	Point group	Raman active	Infrared active	Both Raman- and infrared-active	Silent
Pbam-32	D_{2h}	$16A_g+16B_{1g}+8B_{2g}+8B_{3g}$	$7B_{1u}+15B_{2u}+15B_{3u}$		$8A_u$
$P6/mmm$	D_{6h}	$6A_{1g}+6E_{1g}+12E_{2g}$	$3A_{2u}+11E_{1u}$		$2A_{1u}+6A_{2g}+4B_{1g}+6B_{1u}+2B_{2g}+6B_{2u}+6E_{2u}$
$I\bar{4}3d$	T_d	$11A_1+23E$		$35T_2$	$12A_2+35T_1$

3.2. Calculated Raman spectrum and infrared intensity

In order to investigate Raman spectra, we firstly calculate their non-resonant Raman activities with DFT and list them in Table 3. After that, the first-order non-resonant differential Raman cross section of the stocks component is calculated from the following equation:[44]

$$\frac{\mathrm{d}\sigma}{\mathrm{d}\Omega} = \left(\frac{2h\pi^2}{c^4}\right)\left|\hat{e}_\mathrm{s}\frac{\partial\tilde{\alpha}}{\partial Q}\hat{e}_\mathrm{I}\right|^2\frac{(\nu_\mathrm{i}-\nu_\mathrm{p})^4}{\nu_\mathrm{p}} \times\left(1+\frac{1}{\exp(h\nu_\mathrm{p}/kT)-1}\right), \quad (1)$$

where $\hat{e}_\mathrm{I}$ and $\hat{e}_\mathrm{s}$ are the electric field unit vectors of incident light and scattered light, respectively, $\tilde{\alpha}$ is the polarizability tensor, ν_p and Q are the phonon frequency and its normal-mode coordinate, respectively, ν_i and $(\nu_\mathrm{i}-\nu_\mathrm{p})$ are the incident light frequency and scattered light frequency, respectively, and the last term on the right-hand side, $1+[\exp(h\nu_\mathrm{p}/kT)-1]^{-1}$ is the Bose–Einstein statistical factor, in which T is the temperature. According to the above equation, we show the Raman spectrum at 300 K with 532-nm excitation light in Fig. 2. As the Raman spectrum of diamond usually serves as an external standard,[45] we give the Raman spectrum of diamond at the last line of Fig. 2.

Table 3. Calculated values of frequency (Freq, in unit cm^{-1}) and Raman activity (R.A., in units $\mathrm{Å}^4$/amu) of Raman-active mode.

Pbam-32			1234	B_{1g}	235.4	1329	E_{2g}	0.34	1040	A_1	170
Freq	Sym	R.A.	1244	B_{2g}	15.4	1357	A_{1g}	34.9	1053	T_2	64.2
418	B_{3g}	4×10^{-4}	1283	B_{3g}	4.4	*$I\bar{4}3d$*			1077	T_2	164
441	A_g	2.5	1290	A_g	288.7	Freq	Sym	R.A.	1080	E	0.46
451	B_{2g}	0.15	1303	B_{1g}	82.2	445	A_1	2.0	1085	T_2	26.2
465	B_{1g}	0.017	1305	A_g	158.5	473	T_2	2.9×10^{-2}	1095	A_1	22.6
469	A_g	7.5	1309	B_{3g}	329.7	484	T_2	9.0×10^{-3}	1117	T_2	8.0
489	B_{3g}	0.12	1310	B_{2g}	56.4	516	E	4.2×10^{-3}	1126	E	0.78
505	B_{2g}	2.6×10^{-3}	1312	B_{1g}	15.4	527	T_2	0.55	1131	T_2	70.3
594	A_g	3.4	1336	A_g	60.2	535	E	0.13	1110	T_2	6.8
671	B_{3g}	2.6×10^{-3}	1361	B_{1g}	82.9	569	E	0.58	1144	E	0.83
672	B_{2g}	0.11	1462	A_g	107.6	616	T_2	2.7	1156	A_1	186
675	B_{1g}	1.3×10^{-2}	1464	B_{1g}	11.2	631	T_2	2.8×10^{-2}	1163	E	0.51
688	B_{1g}	1.8×10^{-2}	*P6/mmm*			657	T_2	2.9	1168	T_2	240
709	B_{2g}	0.15	Freq	Sym	R.A.	692	E	1.4×10^{-3}	1176	T_2	2.1×10^{-2}
710	B_{1g}	2.5	360	E_{1g}	8.2×10^{-2}	702	A_1	1.9	1196	E	19.5
747	B_{3g}	2.2×10^{-2}	408	E_{2g}	0.14	710	T_2	0.55	1201	A_1	386
788	A_g	10.0	581	E_{1g}	1. 1	723	T_2	5.1	1216	T_2	53.1
795	B_{1g}	3.8	584	E_{2g}	4.8×10^{-2}	734	E	1.3×10^{-3}	1223	E	5.8
847	A_g	30.8	617	E_{1g}	3×10^{-4}	759	T_2	15.7	1225	T_2	72.7
903	B_{1g}	1.7	631	A_{1g}	6.0	773	A_1	1.1	1239	E	10.7
989	B_{1g}	0.26	652	E_{2g}	15.2	780	E	5.4	1251	T_2	191
1001	A_g	178.3	744	E_{2g}	9.0×10^{-2}	788	T_2	8.3×10^{-2}	1257	E	98.4
1059	A_g	15.9	865	A_{1g}	93.7	819	T_2	3.6	1269	T_2	10. 3
1093	A_g	11.3	926	E_{2g}	3.4	827	T_2	13.2	1276	T_2	3.0
1107	B_{3g}	29.9	1029	A_{1g}	134	865	T_2	29.1	1277	A_1	39.7
1113	B_{1g}	81.1	1059	E_{2g}	11.9	874	A_1	18.6	1277	E	13.4
1130	B_{1g}	7.0	1141	E_{1g}	7.4	880	E	0.86	1289	T_2	171
1143	A_g	73.2	1154	E_{2g}	37.2	910	T_2	5.3	1293	E	86.4
1154	B_{2g}	0.44	1200	A_{1g}	32.1	923	E	0.95	1304	T_2	20.9
1173	A_g	51.0	1205	E_{2g}	0.34	932	E	3. 9	1319	A_1	11.8
1176	B_{1g}	79.1	1222	E_{1g}	96.7	953	E	1.9×10^{-2}	1320	E	2.9
1186	B_{2g}	2.7	1228	E_{1g}	6.7	979	T_2	42.6	1321	T_2	18.2
1190	B_{3g}	100.5	1236	E_{2g}	0.14	995	A_1	269	1328	T_2	199
1202	A_g	16.9	1280	A_{1g}	422	998	E	23.6	1334	T_2	4.0×10^{-3}
1207	B_{1g}	3.7	1295	E_{2g}	65.3	999	T_2	90.5	1345	E	0.46
1226	A_g	257.7	1314	E_{2g}	116	1038	T_2	286			

The Raman spectra in Fig. 2 can be divided into two parts: the left middle frequency range below 1150 cm^{-1} and the right high frequency range above 1150 cm^{-1}. Except for diamond, the other 3 carbon allotropes have obvious peaks in the middle frequency range. The Raman spectrum of *Pbam*-32, $P6/mmm$, and $I\bar{4}3d$ look more complicated than that of Bct-C4, C-carbon, F-carbon, M-carbon, O-carbon, P-carbon, T12, W-carbon, X-carbon, and Z-carbon.[23] It originates from the atom number of primitive unit cell. It is 2 atoms in diamond, 4 atoms in Bct-C4, 8 atoms in F-carbon, M-carbon, and Z-carbon, 12 atoms in C-carbon and T12, and 16 atoms in O-carbon, P-carbon, W-carbon, and X-carbon. However, it is as large as 32 atoms in *Pbam*-32, 36 atoms in $P6/mmm$, and even 94 atoms in *Ibar*43*d*. The larger the atom number, the more the peaks in its Raman spectrum are.

Unlike diamond, these three newly proposed carbon allotropes have infrared active modes. Infrared intensity is proportional to $|\partial\boldsymbol{\mu}/\partial Q|^2$, where $\boldsymbol{\mu}$ is the electric dipole moment and Q is the normal-mode coordinate.[44] The infrared spectrum of carbon nanotube,[30] graphite,[31] graphene,[32] and even diamond under electric field[33] have been reported in experiment. As *Pbam*-32, $P6/mmm$, and $I\bar{4}3d$ are sp^3 carbon allotropes, their Born effective charges[46] are rather small, resulting in low infrared intensity. As given in Table 4, the largest infrared intensity is 0.82 $(D/Å)^2/amu$ for 1352 cm^{-1} of *Pbam*, 0.77 $(D/Å)^2/amu$ for 1125 cm^{-1} of $P6/mmm$, and 0.70 $(D/Å)^2/amu$ for 1117 cm^{-1} of $I\bar{4}3d$. They are much smaller than that of ionic crystals.[41] This indicates that the infrared spectrum may play a key role in identifying newly proposed carbon allotropes.

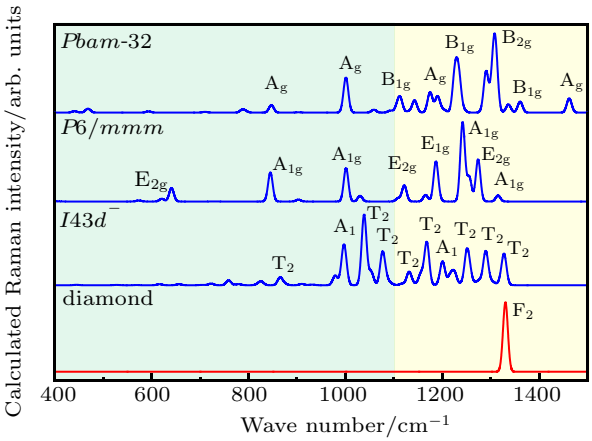


Fig. 2. Calculated Raman spectra of powder sample at 300 K with 532-nm excitation light. There are obvious peaks in the middle frequency region from 600 cm^{-1} to 1150 cm^{-1} except for diamond.

Table 4. Calculated frequency and infrared intensity (I.I., in units $(D/Å)^2/amu\times10^{-2}$) of infrared-active mode.

Pbam-32			1166	B_{2u}	21	1047	E_{1u}	0.04	865	T_2	1.2
Freq	Sym	I.I.	1189	B_{2u}	22	1079	A_{2u}	0.18	910	T_2	14
374	B_{3u}	0.20	1194	B_{3u}	8.5	1084	E_{1u}	4.1	979	T_2	0.23
403	B_{2u}	2.6	1210	B_{2u}	0.07	1125	E_{1u}	77	999	T_2	4.0
544	B_{2u}	0.01	1214	B_{1u}	23	1185	A_{2u}	17	1038	T_2	24
559	B_{1u}	4.2	1215	B_{2u}	1.8	1259	E_{1u}	8.7	1053	T_2	2.0
575	B_{1u}	2.1	1227	B_{3u}	16	1284	E_{1u}	5.8	1077	T_2	27
586	B_{3u}	0.35	1235	B_{1u}	3.5	1311	E_{1u}	5.6	1085	T_2	23
613	B_{2u}	0.71	1257	B_{3u}	4.8	1330	E_{1u}	0.19	1117	T_2	70
657	B_{3u}	1.8	1260	B_{1u}	2.8	*$I\bar{4}3d$*			1131	T_2	0.04
690	B_{1u}	2.1	1271	B_{2u}	14	Freq	Sym	I.I.	1140	T_2	0.69
708	B_{2u}	4.3	1278	B_{3u}	0.25	473	T_2	0.50	1168	T_2	1.7
802	B_{3u}	0.09	1307	B_{3u}	1.1	484	T_2	0.01	1176	T_2	5.4
823	B_{3u}	0.11	1322	B_{2u}	12	528	T_2	2.0	1216	T_2	0.54
874	B_{2u}	4.8	1342	B_{2u}	14	616	T_2	0.17	1225	T_2	2.3
910	B_{2u}	1.1	1352	B_{3u}	82	631	T_2	0.42	1251	T_2	3.3
917	B_{3u}	38	*$P6/mmm$*			657	T_2	5.4	1269	T_2	2.7
934	B_{3u}	0.17	Freq	Sym	I.I.	710	T_2	0.81	1276	T_2	13
1008	B_{2u}	7.4	472	E_{1u}	1.2	723	T_2	1.0	1289	T_2	1.5
1074	B_{3u}	1.9	496	A_{2u}	2.9	759	T_2	2.5	1304	T_2	9.9
1081	B_{1u}	0. 70	692	E_{1u}	0.10	788	T_2	0.01	1321	T_2	2.1
1098	B_{2u}	10	788	E_{1u}	1.6	819	T_2	0.73	1328	T_2	0.50
1117	B_{3u}	9.4	966	E_{1u}	3.2	827	T_2	0.02	1334	T_2	46

3.3. Vibrational modes of principle peaks

As shown in Fig. 2, there are many peaks in the Raman spectra of *Pbam*-32, $P6/mmm$, and $I\bar{4}3d$. In order to give a detailed analysis, we depict the vibrational modes of principle peaks in Figs. 3–5.

Figure 3 shows the vibrational modes of the principle peaks of *Pbam*-32. Based on the atom movement directions, the vibrational modes can be divided into two groups. In Fig. 3(g), 3(m), and 3(n) belong to the first group, in which atoms move along the $\boldsymbol{a}_3$ direction. In Fig. 3(g), the center carbon atoms of most tetrahedrons move in the same direction as one apical carbon atom and opposite to the other two apical atoms. Therefore, its frequency is relatively low. In

Figs. 3(m) and 3(n), the central carbon atoms of most tetrahedrons move opposite to the three apical carbon atoms. They are similar to the F_2 mode of diamond. Therefore, their vibrational frequencies (1309 cm^{-1} for Fig. 3(m) and 1310 cm^{-1} for Fig. 3(n)) are close to the vibrational frequency of diamond F_2 mode (1333 cm^{-1}). The others belong to the second group, in which atoms move in the $\boldsymbol{a}_1$ and $\boldsymbol{a}_2$ planes. In Fig. 3(c), the center (corner) atom pairs of the unit cell move in the opposite directions, and the contributions of other atoms are small. In Fig. 3(d), the contributions of center and corner atom pairs of the unit cell still dominate the mode. The contributions of other atoms increase relative to the scenario in Fig. 3(c). In Fig. 3(e), carbon atoms move almost along the $\boldsymbol{a}_2$ direction, and most atoms move opposite to their nearest neighbors. The vibrational modes of Figs. 3(o)–3(q) are dominated by a few specific atom pairs.

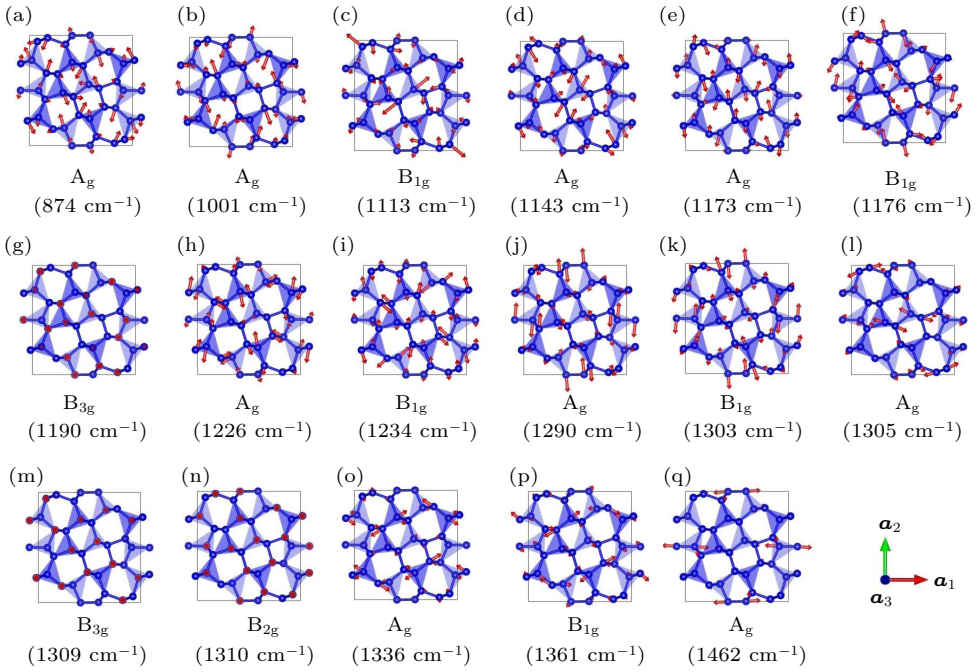


Fig. 3. Vibrational modes of principle peaks of *Pbam*-32.

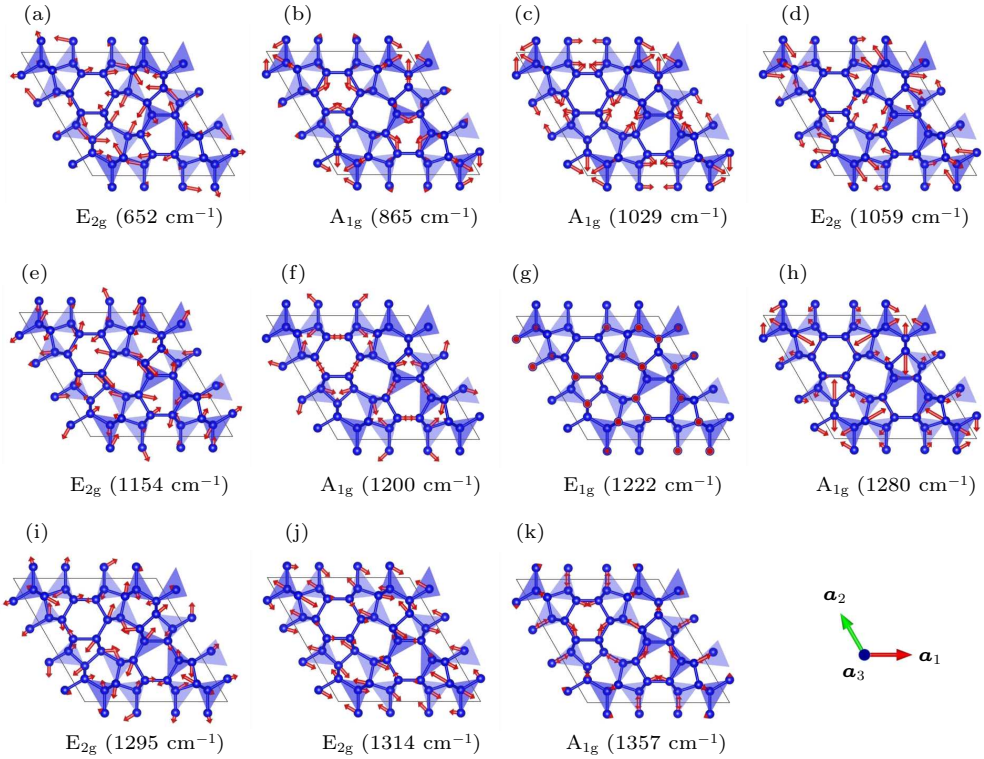


Fig. 4. Vibrational modes of principle peaks of *P*6/*mmm*.

As $P6/mmm$ has six-fold symmetry, the vibrational modes in Fig. 4 look more regular than those in Fig. 3. In Fig. 4(g), all atoms move along the $\boldsymbol{a}_3$ direction. The mode in Fig. 4(g) is similar to the vibrational mode of Fig. 3(g). Except for the mode in Fig. 4(g), the other modes in Fig. 4 vibrate in the $\boldsymbol{a}_1$ and $\boldsymbol{a}_2$ planes. In Figs. 4(b), 4(c), and 4(h), the regular sixfold carbon rings in the unit cell corners vibrate like a breathing mode:[23,29] all atoms of the sixfold ring move toward the ring center. In Fig. 4(b), the regular sixfold carbon rings both at four corners and in the center of the unit cell vibrate in phase like a breathing mode. In Fig. 4(c), the regular sixfold rings at the corners and the eightfold rings in the center of unit cell vibrate in phase like a breathing mode. In Fig. 4(f), the atoms of the regular sixfold rings vibrate toward each other. It is similar to the fully symmetric vibrational mode of graphene at K point. The vibrational mode of Fig. 4(k) looks similar to Fig. 4(f). In Fig. 4(k), it is the atoms of eightfold rings that vibrate toward each other, which differs from the atoms of the sixfold rings in Fig. 4(f). In Fig. 4(j), the center atoms in most of tetrahedrons move opposite to their apical atoms. It is similar to the F_2 mode of diamond. Therefore, its vibrational frequency (1314 cm^{-1}) is close to that of diamond (1333 cm^{-1}).

The vibrational modes of $I\bar{4}3d$ depicted in Fig. 5 are complicated. Although $I\bar{4}3d$ belongs to the high-symmetry point group T_d, there are 94 carbon atoms in its primitive unit cell. Consequently, the vibrational modes depicted in Fig. 5 are complicated and irregular. They do not show clear and distinct pattern. All the detailed information about vibrational modes of *Pbam*-32, $P6/mmm$, and $I\bar{4}3d$ can be found in supplementary data.

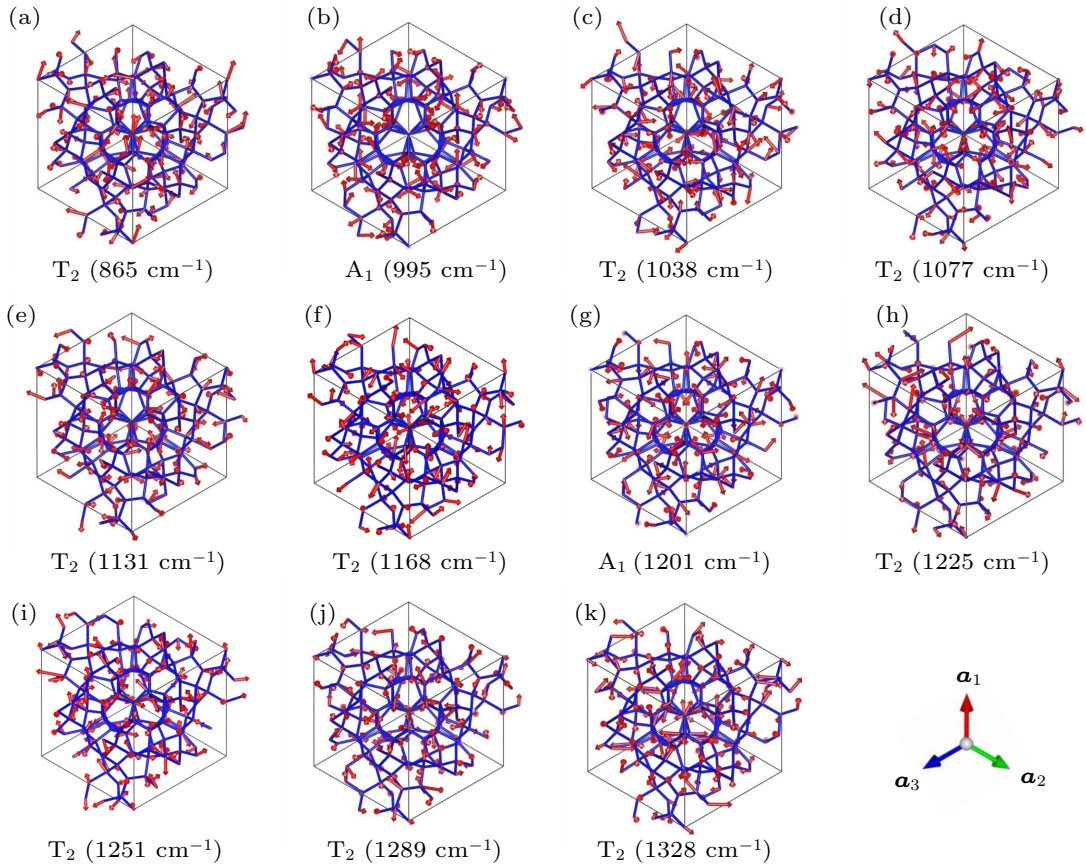


Fig. 5. Vibrational modes of principle peaks for $I\bar{4}3d$. We only give carbon wireframe here for clarity.

3.4. Electronic band structures

In order to to deepen the understanding of these three new carbon allotropes, we calculate their electronic band structures and show them in Fig. 6. As shown in Fig. 6, the *Pbam*-32, $P6/mmm$, and $I\bar{4}3d$ have obvious band gaps, which are 4.8, 3.4, and 6.1 eV, respectively. For the occupied states from -21 to 0, they are composed of 2s and 2p states. Owing to the sp^3 bonds, there are obvious energy dispersion in Figs. 6(a)–6(c). Compared with Figs. 6(a) and 6(b), figure 6(c) is a little messy. This is because there are 32 atoms in the primitive unit cell of *Pbam*-32, 36 atoms in $P6/mmm$, and 94 atoms in $I\bar{4}3d$. The atom number in $I\bar{4}3d$ is about three times that of *Pbam*-32 and $P6/mmm$. This large number of atoms brings about the fact that there are more points in the band structure of $I\bar{4}3d$ for a special k point.

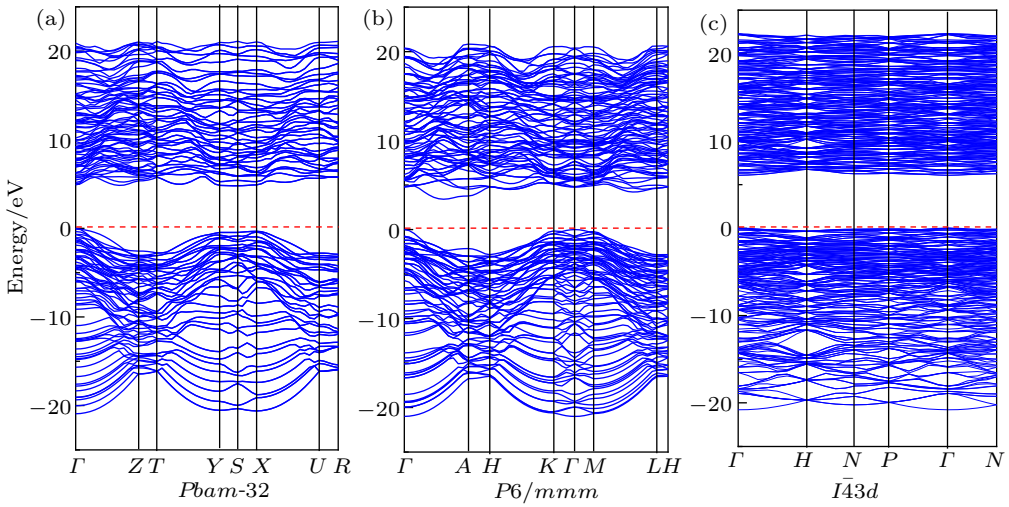


Fig. 6. Calculated electronic band structures of (a) *Pbam*-32, (b) *P*6/*mmm*, and (c) $I\bar{4}3d$. The energy of the highest occupied state is set to be zero.

4. Conclusions

By the factor group analysis method, we classify the vibrational modes as *Pbam*-32, *P*6/*mmm*, and $I\bar{4}3d$. Owing to the large atom numbers in their primitive unit cells, these three carbon allotropes have many Raman and infrared active modes. There are 48 Raman-active modes ($16A_g+16B_{1g}+8B_{2g}+8B_{3g}$) and 37 infrared-active modes ($7B_{1u}+15B_{2u}+15B_{3u}$) in *Pbam*-32, 24 Raman-active modes ($6A_{1g}+6E_{1g}+12E_{2g}$) and 14 infrared-active modes ($3A_{2u}+11E_{1u}$) in *P*6/*mmm*, and 34 Raman-active modes ($11A_1+23E$) and 35 Raman- and infrared-active modes ($35T_2$) in $I\bar{4}3d$. After that, we calculate their Γ-point phonon frequencies. We find that most of frequencies of the Raman-active modes are far below the Raman frequency of diamond (1333 cm^{-1}) and graphite (1350 cm^{-1} and 1586 cm^{-1}). Furthermore, we calculate the first-order Raman and infrared intensities. Their Raman spectra can be divided into two ranges: middle frequency range from 600 cm^{-1} to 1150 cm^{-1} and high frequency range above 1150 cm^{-1}. Their largest infrared intensities are 0.82, 0.77, and 0.70 $(D/Å)^2$/amu for *Pbam*-32, *P*6/*mmm*, and $I\bar{4}3d$, respectively. This indicates that the middle frequency Raman shift and infrared spectrum may play a key role in identifying newly proposed carbon allotropes.

Acknowledgement

The crystal structure was drawn using the VESTA software.[47]

References

[1] Hoffmann R, Kabanov A A, Golov A A and Proserpio D M 2016 *Angewandte Chemie International Edition* **55** 10962

[2] Cao Y, Fatemi V, Demir A, Fang S, Tomarken S L, Luo J Y, Sanchez-Yamagishi J D, Watanabe K, Taniguchi T and Kaxiras E 2018 *Nature* **556** 80

[3] Cao Y, Fatemi V, Fang S, Watanabe K, Taniguchi T, Kaxiras E and Jarillo-Herrero P 2018 *Nature* **556** 43

[4] Takagi M, Taketsugu T, Kino H, Tateyama Y, Terakura K and Maeda S 2017 *Phys. Rev. B* **95** 184110

[5] Shi X, He C, Pickard CJ, Tang C and Zhong J 2018 *Phys. Rev. B* **97** 014104

[6] Oganov A R and Glass C W 2006 *J. Chem. Phys.* **124** 244704

[7] He C, Shi X, Clark S J, Li J, Pickard C J, Ouyang T, Zhang C, Tang C and Zhong J 2018 *Phys. Rev. Lett.* **121** 175701

[8] He C, Zhang C, Xiao H, Meng L and Zhong J 2017 *Carbon* **112** 91

[9] Ribeiro F J, Tangney P, Louie S G and Cohen M L 2006 *Phys. Rev. B* **74** 172101

[10] Li Q, Ma Y, Oganov A R, Wang H, Wang H, Xu Y, Cui T, Mao H K and Zou G 2009 *Phys. Rev. Lett.* **102** 175506

[11] He C, Sun L, Zhang C, Peng X, Zhang K and Zhong J 2012 *Solid State Commun.* **152** 1560

[12] Li D, Bao K, Tian F, Zeng Z, He Z, Liu B and Cui T 2012 *Phys. Chem. Chem. Phys.* **14** 4347

[13] Sheng X L, Yan Q B, Ye F, Zheng Q R and Su G 2011 *Phys. Rev. Lett.* **106** 155703

[14] Zhang J, Wang R, Zhu X, Pan A, Han C, Li X, Zhao D, Ma C, Wang W and Su H 2017 *Nat. Commun.* **8** 683

[15] Yang X, Yao M, Wu X, Liu S, Chen S, Yang K, Liu R, Cui T, Sundqvist B and Liu B 2017 *Phys. Rev. Lett.* **118** 245701

[16] Amsler M, Flores-Livas J A, Lehtovaara L, Balima F, Ghasemi S A, Machon D, Pailhès S, Willand A, Caliste D, Botti S, San Miguel A, Goedecker S and Marques M A L 2012 *Phys. Rev. Lett.* **108** 065501

[17] Mao W L, Mao H K, Eng P J, Trainor T P, Newville M, Kao C C, Heinz D L, Shu J, Meng Y and Hemley R J 2003 *Science* **302** 425

[18] Shi S, Gao J, Liu Y, Zhao Y, Wu Q, Ju W, Ouyang C and Xiao R 2016 *Chin. Phys. B* **25** 018212

[19] Gupta A, Chen G, Joshi P, Tadigadapa S and Eklund PC 2006 *Nano Lett* **6** 2667

[20] Tan P H, Han W P, Zhao W J, Wu Z H, Chang K, Wang H, Wang Y F, Bonini N, Marzari N, Pugno N, Savini G, Lombardo A and Ferrari A C 2012 *Nat. Mater.* **11** 294

[21] Lui C H and Heinz T F 2013 *Phys. Rev. B* **87** 121404

[22] Ferrari A C, Meyer J, Scardaci V, Casiraghi C, Lazzeri M, Mauri F, Piscanec S, Jiang D, Novoselov K and Roth S 2006 *Phys. Rev. Lett.* **97** 187401

[23] Bai Y, Zhao X, Li T, Lv Z, Lv S, Han H, Yin Y and Wang H 2014 *Carbon* **78** 70

[24] Wang H, Wang Y, Cao X, Feng M and Lan G 2009 *J. Raman Spectros.* **40** 1791

[25] Wang H, You J, Wang L, Feng M and Wang Y 2010 *J. Raman Spectros.* **41** 125

[26] Gupta A, Chen G, Joshi P, Tadigadapa S and Eklund P 2006 *Nano Lett.* **6** 2667

[27] Wang H, Feng M, Zhang X, Tan P H and Wang Y 2015 *J. Phys. Chem. C* **119** 6906
[28] Kürti J, Kresse G and Kuzmany H 1998 *Phys. Rev. B* **58** R8869
[29] Wang H, Cao X, Feng M, Wang Y, Jin Q, Ding D and Lan G 2009 *Spectrochim Acta A Mol. Biomol. Spectrosc.* **71** 1932
[30] Tsareva S Y, Devaux X, McRae E, Aranda L, Gregoire B, Carteret C, Dossot M, Lamouroux E, Fort Y, Humbert B and Mevellec J Y 2014 *Carbon* **67** 753
[31] Nemanich R J, Lucovsky G and Solin S A 1997 *Solid State Commun.* **23** 117
[32] Li Z Q, Henriksen E A, Jiang Z, Hao Z, Martin M C, Kim P, Stormer H L and Basov D N 2008 *Nat. Phys.* **4** 532
[33] Anastassakis E and Burstein E 1970 *Phys. Rev. B* **2** 1952
[34] Giannozzi P, Baroni S, Bonini N, Calandra M, Car R, Cavazzoni C, Ceresoli D, Chiarotti G L, Cococcioni M, Dabo I, Dal Corso A, de Gironcoli S, Fabris S, Fratesi G, Gebauer R, Gerstmann U, Gougoussis C, Kokalj A, Lazzeri M, Martin-Samos L, Marzari N, Mauri F, Mazzarello R, Paolini S, Pasquarello A, Paulatto L, Sbraccia C, Scandolo S, Sclauzero G, Seitsonen AP, Smogunov A, Umari P and Wentzcovitch RM 2009 *J. Phys.: Condens. Matter* **21** 395502
[35] Troullier N and Martins J L 1991 *Phys. Rev. B* **43** 1993
[36] Baroni S, de Gironcoli S and Dal Corso A 2001 *Rev. Mod. Phys.* **73** 515
[37] Feng X K, Shi S, Shen J Y, Shang S L, Yao M Y and Liu Z K 2016 *J. Nucl. Mater.* **479** 461
[38] Shi S, Ke X, Ouyang C, Zhang H, Ding H, Tang Y, Zhou W, Li P, Lei M and Tang W 2009 *J. Power Sources* **194** 830
[39] Shang S L, Hector J L G, Shi S, Qi Y, Wang Y and Liu Z K 2012 *Acta Materialia* **60** 5204
[40] Shi S, Zhang H, Ke X, Ouyang C, Lei M and Chen L 2009 *Phys. Lett. A* **373** 4096
[41] Wang H, Liu H, Zhang Z, Liu Z, Lv Z, Li T, Ju W, Li H, Cai X and Han H 2019 *NPJ Comput. Mater.* **5** 1
[42] Wang H, Kong L, Zhao X, Lv Z, Li T, Ju W W, You J and Bai Y 2013 *Appl. Phys. Lett.* **103** 101902
[43] Zhang G Y, Lan G X and Wang Y F 1991 *Lattice Vibration Spectroscopy*, 2nd edn. (High Education Press) p. 79 (in Chinese)
[44] Porezag D and Pederson M 1996 *Phys. Rev. B* **54** 7830
[45] Favors R N, Jiang Y, Loethen Y L and Ben-Amotz D 2005 *Rev. Sci. Instrum.* **76** 033108
[46] Lü Z L, You J H, Zhao Y Y and Wang H 2011 *Commun. Theor. Phys.* **55** 513
[47] Momma K and Izumi F 2011 *J. Appl. Crystallography* **44** 1272